University of Glasgow

Yousaf, J., Abed, A. M.A., Zia, H., Almajali, E., Tahir, F. A. and Rmili, H. (2023) Robust deep learning-based detection and classification system for chipless Arabic RFID letters. *Engineering Applications of Artificial Intelligence*, 122, 106147. (doi: 10.1016/j.engappai.2023.106147)

This is the author version of the work deposited here under a Creative Commons licence: https://creativecommons.org/licenses/by-nc-nd/4.0/
There may be differences between this version and the published version. You are advised to consult the published version if you wish to cite from it.
https://doi.org/10.1016/j.engappai.2023.106147

https://eprints.gla.ac.uk/294994/

Deposited on: 9 May 2023

Enlighten – Research publications by members of the University of Glasgow
http://eprints.gla.ac.uk

Robust Deep Learning-based Detection and Classification System for Chipless Arabic RFID Letters

Jawad Yousaf[a,*], Abdelrahman M. A. Abed[a], Huma Zia[a], Eqab Almajali[b], Farooq A. Tahir[c,d] and Hatem Rmili[e]

[a]Department of Electrical, Computer, and Biomedical Engineering, Abu Dhabi University, Abu Dhabi, 1970, United Arab Emirates
[b]Department of Electrical Engineering, University of Sharjah, Sharjah, 27272, United Arab Emirates
[c]James Watt School of Engineering, University of Glasgow, Glasgow, G12 8QQ, United Kingdom
[d]School of Electrical Engineering and Computer Science, National University of Sciences and Technology (NUST), Islamabad, 44000, Pakistan
[e]Electrical and Computer Engineering Department, Faculty of Engineering, King Abdulaziz University, Jeddah, 21589, Saudi Arabia

ARTICLE INFO

Keywords:
Deep Learning
Alphabet RFID
Chipless RFID
Arabic Letter RFID
LSTM

ABSTRACT

This work demonstrates a novel approach for reliable and robust identification and detection of realized chipless RFID Arabic alphabets using deep learning (DL) method. The undertaken classification problem of Arabic RFID tags of various fonts and sizes requires a classification technique that can learn long-term dependencies. Hence, a Bi-Long Short-Term Memory (BiLSTM) model is developed to classify 28 chipless Arabic RFID letters of different font types and sizes using their back scattered dual-polarized radar cross section (RCS) characteristics. The RCS frequency response of each Arabic letter tag reflects its signature electromagnetic characteristics that vary with the change in its shape (variations in font type and size). Firstly, an RCS dataset of 28 Arabic alphabet tags with three different font types (Arial, Calibri, and Times New Roman) and 13 different font sizes (16 mm - 28 mm with a step size of 1 mm) are generated using Finite-Difference Time-Domain (FDTD) method in the frequency range of 1-12 GHz (1001 steps). The dimensions of the resulting dataset are [28 (letters) x 13 (font sizes) x 1001 (frequency steps) x 2 (polarizations)] x 3 (font types). Multi-class classification of the frequency-series data of all realized 28 alphabet tags of various font types and sizes makes the problem challenging and novel. The developed BiLSTM model can accurately classify the particular letter tag with specific font type and size based on the optimized network with employed Leave-One-Out Cross-Validation (LOOCV). The achieved accuracy with only Arial ($[(28 \times 13 \times 1001 \times 2)]$), Calibri ($[(28 \times 13 \times 1001 \times 2)]$), Times New Roman ($[(28 \times 13 \times 1001 \times 2)]$), and combined data set ($[(28 \times 13 \times 1001 \times 2)] \times 3$) is 75%, 74%, 75%, and 89% respectively. The proposed Bi-LSTM model is shown superior when compared to other methods such as SVM, decision trees, and KNN, as it classifies the data with much higher accuracy for the considered multi-class data. The obtained accuracies of the compared models are 6.4% (SVM), 17.30% (tree) and 27.4% (KNN) respectively, while the developed Bi-LSTM model with optimized hyperparameters achieved an accuracy of 96%.

1. Introduction

Frequency Identification (RFID) and Artificial Intelligence (AI) research have seen an enormous development in the last few years with massive potential in developing Internet of Things (IoT) systems and smart cities [1, 2]. Chipless RFID tags have become very popular because they did not include silicon chip, battery, and antenna on the metallic tag for successful operation. Instead, their characteristics are encoded by the use of the electromagnetic signature (EMS) of the tag, which reduces the cost of the tag and makes it lighter and more compact [3, 4, 5]. The RFID reader of frequency-domain chipless tags can distinguish between each metallic resonant tag based on the reflected signal from the tag that carries the unique EM characteristics for each tag [6, 7, 8].

*This research work was funded by Institutional Fund Projects under grant no. (IFPIP-381-135-1443). Therefore, the authors gratefully acknowledge technical and financial support from the Ministry of Education and King Abdulaziz University, Jeddah, Saudi Arabia. Also, this work was supported by Abu Dhabi University's Office of Research and Sponsored Programs.

*Corresponding author
jawad.yousaf@adu.ac.ae (J. Yousaf); 1063674@students.adu.ac.ae (A. M.A. Abed); huma.zia@adu.ac.ae (Huma Zia); ealmajali@sharjah.ac.ae (Eqab Almajali); farooq.tahir@glasgow.ac.uk (Farooq A. Tahir); hmrmili@kau.edu.sa (H. Rmili)
ORCID(s):

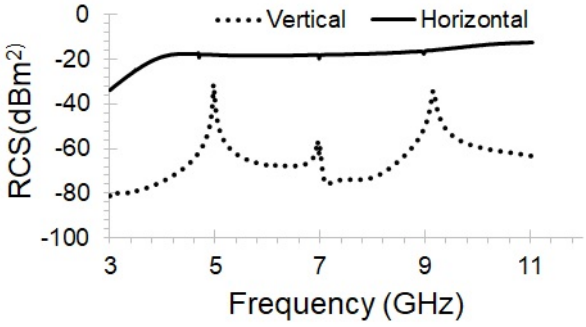

Figure 1: Typical RCS electromagnetic signature of a chipless Arabic letter tag

Table 1
Summary of compared studies of conventional methods for chipless RFID letters detection

Reference	Year	Tag Type	Font Type	Font Size	Tag Size (mm^2)	Detection Method	Frequency (GHz)
Vena [25]	2011	26 Latin alphabet	Arial	48mm	45x48	A look up table for all RCS signatures	3.1- 10.6
Singh [19]	2011	26 Latin alphabet	Arial	24 mm	–	Observing the resonant peaks in S_{11}	1-10
Aminul[4]	2012	4 Rectangular metallic patches	–	Different sizes	–	*S* parameters of the back-scattered signal	7–12
Khaled [26]	2018	10 L-shaped resonators	–	Different sizes	–	Correlation features in the frequency content of the back-scattered signals	6.5 -10.5
Boularess[27]	2019	3 Latin Alphabet (a, b , c)	Arial	15 mm	40x20	RCS resonant frequency lookup table of the tags	6-13
Hatem.[6]	2019	3 Latin Alphabet (a, b , c)	Arial Corbel Times New Roman	Different sizes	40x20	Frequency shift analysis of tags RCS response.	6-13
Boularess [28]	2019	18 Arabic alphabets	Arial	24 mm	37x37	RCS resonant frequency lookup table of the tags	2-8
Wazie [29]	2018	6 Multiresonating circuit	–	–	33.13 x10.225	Dips in S_{21} and S_{11} of the proposed tags	6.1-6.6

The frequency-domain chipless tags are available in the form of different geometrical shaped- and letter-based resonators. Some examples of foremost category are tags based on split ring resonators [9, 10]; M/U/T/E-Shaped strips [11, 12]; slotted patch [13]; nested square loops [14]; space-filling curve shape [15]; slot/stub-loaded patches [16]; and multi-layer patches [17].

Alphabet-based chipless RFID tags are being developed for the attractive applications in document security, products advertisement, health, and inventory management [18, 6]. Both Latin [19**?** , 7] and Arabic[18, 20, 21] alphabet tags are reported in the open literature. The realised metallic tag-name based on alphabets could be used as an RFID tag and thus reduce the need for the installation of separate bar-codes or conventional resonators. The other advantage of such tags is using them for visual identification [22, 7].

The spectral resonances (electromagnetic signature (EMS)) from the back scattered response of frequency-domain tags are analyzed for their encoding. The convectional approaches involves the analysis of the peaks/dips in the recorded back scattered *S*-parameters [7, 19, 12], electric-field [21], and radar cross section (RCS) characteristics [18, 6, 20, 23, 24] of designed tags. Figure 1 shows the typical co- and cross-polar RCS characteristics of a chipless Arabic RFID letter tag. The difference in the number of resonances or resonance frequencies in recorded EMS is used to classify the different analyzed tags in [7, 19, 12, 21, 18].

Hybrid encoding techniques based on magnitude, phase, and frequency shift coding of observed EMS are also proposed to enhance the coding capacity of the tags [6, 14, 23]. A look-up table based approach is also reported for the identification of different analyzed Arabic [21, 20, 18] and Latin [6, 19, 7] alphabets-based tags. In this approach, the obtained resonance frequencies in RCS of the realized tags are compared with the already developed look-up tables for its detection and classification. The reviewed recent studies related the chipless RFID tags detection using aforementioned conventional approaches are summarized in Table 1. It has been reported in [20, 18, 6] that any minor change in the metallic letter shape of the realized tag will vary its signature (EMS). The traditional techniques as summarized in Table 1 become cumbersome for the accurate identification and encoding of the tags when the number

Table 2
Comparison of legacy studies using the AI techniques for chipless RFID detection

Reference	Year	Tag Type	Font Type	Font Sizes	Tag Size (mm^2)	Detection Method	Frequency (GHz)	Data Set	Test Accuracy (%)
Larry [7]	2018	5-symbolic	-	-	50 × 10	Machine learning (SVM) on S_{21} parameters	57 - 64	27 Tags combinations	96
Soyeon [11]	2019	4 T-shaped	-	-	40 × 0.5	SVM Classification on S-parameters magnitude/phase data	0 - 10	816 × 500	89.6 - 99.3
Nastasiu [12]	2020	18 E-shape	-	-	21.3 × 9	Neural network model based on EM signature	65 - 72	200 × 18	100
This work	2023	28 Arabic alphabets	Arial, Calibri, Times New Roman	16 mm - 28 mm (step size : 1 mm)	50 × 40	Deep learning using BiLSTM network on co- and cross-polar RSC results	1- 12	[(28 × 13 × 1001 × 2)] × 3	89 (*92 - 96)

of letter tags, tag's combinations or structural variations (like changes in font type, size, and spacing) in the letter-tags increases.

Deep learning algorithms have increasingly become a very effective solution for detecting nonlinear and hierarchical features in image classification, audio and text classification, signal analysis and detection, and object detection. The authors in [30] proposes a novel architecture, Precise Single Stage Detector (PSSD), to address the issues of reduced accuracy and slow processing in object detection. Also, another study by [31] solves the issue of limited and unlabeled data used in semi-supervised learning (SSL) and few shot learning (FSL), by proposing an efficient way of generating pseudo-examples through the generator network only. The model was tested on Urdu digits images for digit detection, and demonstrated improvement over state-of-the-art in average accuracy. In [32], a novel learning framework is presented for multiple graph learning and multi-view semi-supervised classification to address the limitation of existing graph learning neural networks that are mainly developed for single graph data.

Recently, machine learning (ML) techniques are proposed to resolve countered issues by conventional approaches. A cloud-based pattern recognition using support vector machine (SVM) algorithm is reported in [7]. The developed system in [7] analyzed the S_{21} data of the 27 combination of Peyote symbols of five letters for the accurate detection of tag-ID. The authors in [11] also used SVM algorithm on the 816 results of 4 T-shaped 2-bit encoding tags for their detection and classification. Nastasiu *et al.* [12] presents a model based on a neural network that can classify the 18 E-shaped RFID tags based on their EM signatures. Table 2 summarizes the recent AI-based studies for the detection and classification of RFID tags. The compared studies in Table 2 are either for a fixed Latin shape [11, 12] or for combinations of Peyote symbols [7] with limited number of alphabets.

This work proposes, for the first time, a new deep learning based approach for the robust and accurate detection and classification of 28 Arabic letter tags of different fonts and sizes. Chipless Arabic alphabet tags are realized by etching the metallic (copper) letter shape on a cheap paper substrate ($\epsilon_r = 2.31$) of 40 mm × 50 mm [18]. The tags are designed using three different font types (Arial, Calibri, and Times New Roman) and 13 different font sizes (16-28 mm with step size of 1 mm). All tags are illuminated with a plane wave and their back scattered RCS signatures in horizontal and vertical polarizations are predicted using CST Microwave Studio (MWS) in the frequency range of 1-12 GHz with 1001 steps. The peaks and dips in the vertical and horizontal RCS response represent the distinct characteristics of the analyzed letter tag as illustrated in Figure 1. The unique resonances in the RCS spectrum of each letter tag for each font type and size will be used for its detection and identification using the proposed novel deep learning (DL) system. A DL classification technique based on Long Short-Term Memory (LSTM) architecture to read, analyze, and detect chipless Arabic RFID letters is used. Firstly, the obtained RCS dataset ([28 (letters) x 13 (font sizes) x 1001 (frequency steps) x 2 (polarizations)] x 3 (font types) of the designed alphabet tags is passed to the data cleaning process and then inserted into the designed and optimized BiLSTM classifier. The training and testing of the data is performed by conducting eleven different experiments based on the variations in the input dataset and network settings (hyper-parameter optimization) as detailed in Section 3. The achieved accuracy for the detection and classification

of the designed Arabic letter tags with only Arial ([(28 x 13 x 1001 x2)]), Calibri ([(28 x 13 x 1001 x2)]), Times New Roman ([(28 x 13 x 1001 x2)]), and combined data set ([(28 x 13 x 1001 x2)] x 3) is 75%, 74%, 75%, and 89% respectively. The dataset tuning is proved useful in further improving the tags detection and classification accuracy to 92%-96%. The conventional supervised learning models did not perform well for such dataset as the maximum achieved classification accuracies with the compared state of the art techniques such as support vector machine (SVM), decision tree, and k-nearest neighbors (KNN) are 6.4%, 17.3%, and 27.4% respectively. It proves the superiority of the proposed BiLSTM network over the compared networks.

The major contribution of this study are:

- Generating a comprehensive database of RCS responses of 28 Arabic alphabets with 3 different font types and 13 font sizes though full-wave EM simulations
- Proposing a novel approach based on a BiLSTM deep learning framework for the detection and classification of each tag irrespective of its font type and size
- Detailed and comprehensive analysis of classification accuracy with the variations in network type (BiLSTM, KNN, SVM, decision tree), hyperparaemters of BiLSTM network, and input data type for the design of a robust detection system for the promising letter based chipless tags

As per our best knowledge, the proposed approach is the first of its kind for the identification and robust detection of such generated extensive data set of Arabic RFID letter tags. Other than letter tags detection, the proposed approach has potential of application in other area such as converting document images into digital documents, text detection in images, document/cheques security, product advertisements, and also for use in autonomous vehicles to perform license plate reading.

The rest of the paper is organized as follows: Section 2 describes the design procedure and numerical results of all realized 28 Arabic letters of various fonts and sizes. The details of the proposed DL-based detection system is given in Section 3. Section 4 discusses the results of the different designed experiments. The discussion of the overall results is detailed in 5. Lastly, Section 6 concludes the findings of the study.

2. Design Process And Data Generation of Arabic Letter Tags

The data generation process in this work consists of three steps. Step one is the design of each Arabic letter using a 3D design software such as Auto CAD for each realized font type and size. In step two, the drawn tags, obtained in step one, are imported into CST Microwave studio to generate the RCS results based on the full-wave EM simulation of each tag [18]. Finally, the RCS results in both, the horizontal and vertical polarizations, of each tag are imported into MATLAB in order to train and classify the tags during the proposed deep learning network of Figure 16.

2.1. Numerical Analysis

Figure 2 shows the full-wave EM model of the imported alphabet (Alf) أ from the Auto CAD software. Each designed letter is assigned a copper material with a thickness of 0.1 mm and is placed on a paper substrate of 40 mm

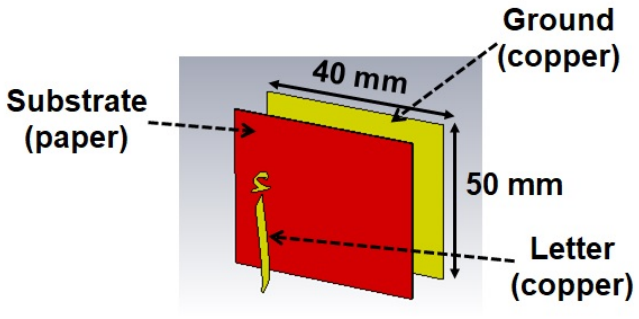

Figure 2: Structure and dimensions of designed Arabic letter tags (example of letter (Alf) أ)

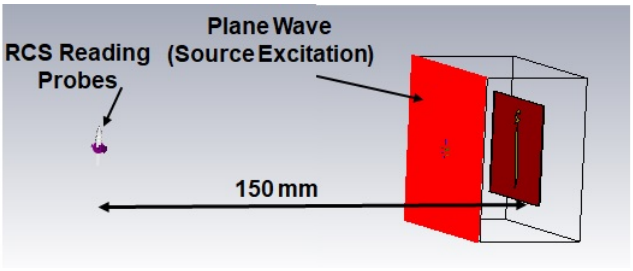

Figure 3: Full-wave numerical analysis setup for realized Arabic letter tags

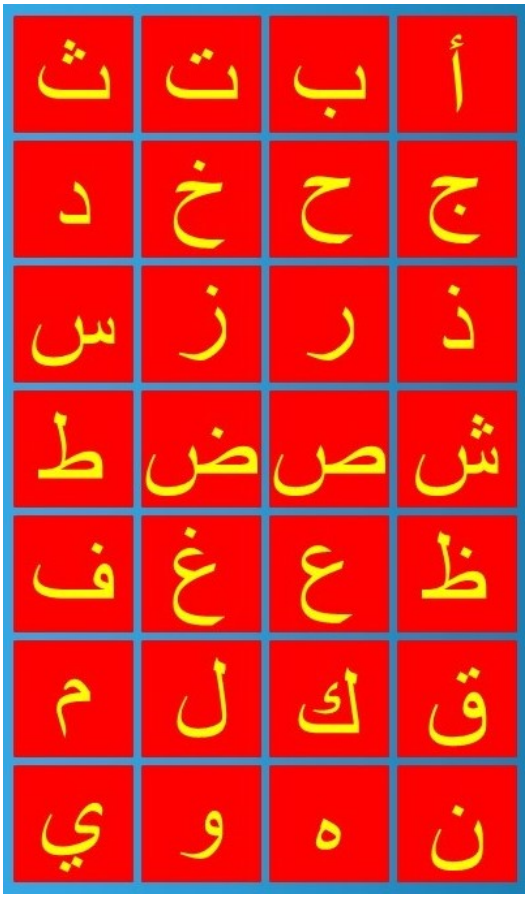

Figure 4: All designed Arabic letter-tags with Times New Roman font type with font size of 28 mm

× 50 mm with a height of 0.5 mm. A copper ground plane is inserted at the bottom of the substrate as shown in Figure 2. Each letter tag should be located at the center of the substrate plane.

The realized letter tag is then illuminated with a plane wave which causes the metallic letter geometry to resonate. Figure 3 shows the full-wave EM analysis setup for all designed Arabic letter tags. As shown, E-field probes are placed in the far-field region, at a distance of 150 mm from the tag surface , to measure the back scattered RCS waveform in both the co-and cross-polarization [18]. The RCS responses are predicted and analyzed at many frequencies in the frequency range from 1 to 12 GHz . The validity of the utilized numerical setup is established through a rigorous analysis reported in [18]. The dips and peaks in the recorded RCS results depict the EM signature properties of a particular tag and the EM signature is found sensitive to any change in the geometrical properties of the tags . Each

Arabic letter shape is different as illustrated in Figure 4 for the realized tag based on Times New Roman (TNR) font of size 28 mm. The induced current distribution on the metallic tag surfaces varies with the change in its geometrical shape and hence produces a unique EM signature of each Arabic letter tag [18, 20]. It has been proven in our earlier study [18] that for a fixed font type and size, each Arabic letter tag has a distinct EM response that effectively identifies the letter to the reader .

2.2. Effects of Changing the Font Size

The change in font size leads to a change on the tag structure . The structural variation will vary the resultant RCS response as it definitely affects the current distribution on the tag's surface . To investigate the effect of changing the font size on the RCS results, three font types are considered namely, the Arial, the Calibri, and the Times New Roman (TNR). For each of the font types, 13 font sizes will be considered to analyze the impact of changing the font type and sizes on the signature EMS of all 28 Arabic letter tags. Firstly, the impact of changing the font size is discussed for a fixed font type. For the Arial type, the font sizes used are 16 mm, 17 mm, 18 mm, 19 mm, 20 mm, 21 mm, 22 mm, 23 mm, 24 mm, 25 mm, 26 mm, 27 mm, and 28 mm respectively. Figure 5 shows how the tag size for the Arabic letter (Alf) أ changes when changing the font size from 16 to 28 for a fixed Arial font type.

The RCS results in the vertical polarization for the tags shown in Figure 5 are depicted in Figure 6. All Arabic letter tags shows prominent RCS peaks in the vertical polarization [18] and that's why only vertical polarization RCS waveforms of the discussed tags are reported here for brevity. However, both the horizontal and vertical RCS waveforms

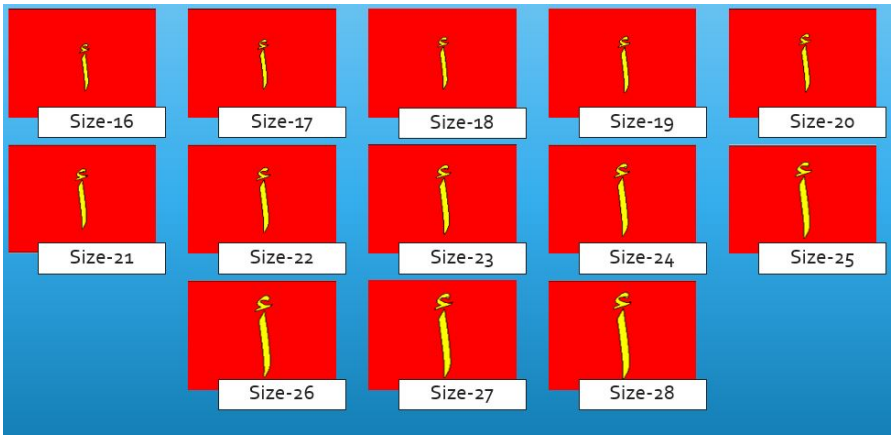

Figure 5: Alf (أ) tag in Arial font type with font size variation from 16 mm to 28 mm

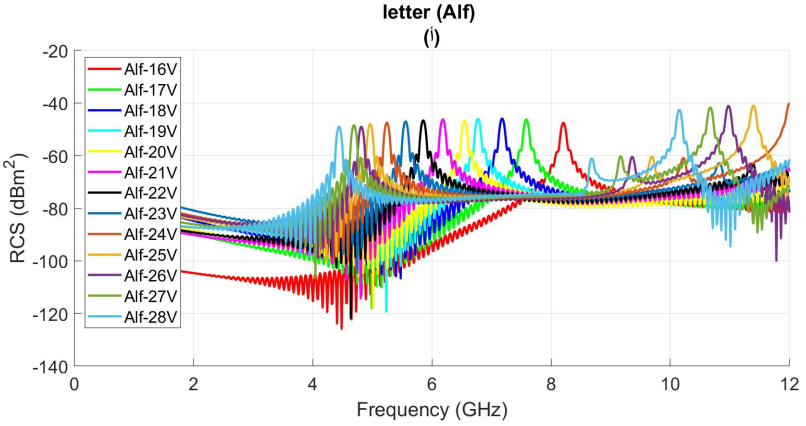

Figure 6: Cross polar RCS results of letter tag Alf (أ) for Arial font type in different sizes

data is used in the detection and classification process of the deep learning system discussed later . From results depicted in Figure 7, one can easily observe three distinguishable peaks at 4.432 GHz, 8.678 GHz and 10.150 GHz,respectively, for the letter tag Alf (أ) with a font size of 28 mm. These resonance peak frequencies shift to 4.696 GHz, 9.162 GHz and 10.670 GHz when the font size is decreased to 27mm . It can be noted from the comparison of all responses shown in Figure 6 that the reduction of the tag's electrical size ,through decreasing the font size, shifts its resonance peaks towards higher frequencies .

In the second illustrating example, Calibri font type is chosen and the font size of alphabet Alf (أ) is varied to study the effect of changing the font size on the the letter tag's EMS . Figure 7 shows the RCS results of letter (أ) for Calibri font type with 13 different sizes for the vertical polarization . The observed signature resonance of the letter أ tag with font size of 28 mm are 4.069 GHz, 6.742 GHz, 7.919 GHz and 11.440 GHz respectively. These resonance peaks change to 4.33 GHz, 7.171 GHz, and 8.425 GHz respectively for the same letter tag when the font size is decreased to 27 mm . We learned from the RCS results in Figure 7 that when the font size decreases, the resonances shift up (to the right as revealed by Figure 7).

The same procedure is repeated for all Arabic alphabet tags by fixing the font type while varying the font size in the range form 16 mm to 28 mm. Figure 8 depicts the cross polar RCS results of letter tag Aen (ع) for Arial font type

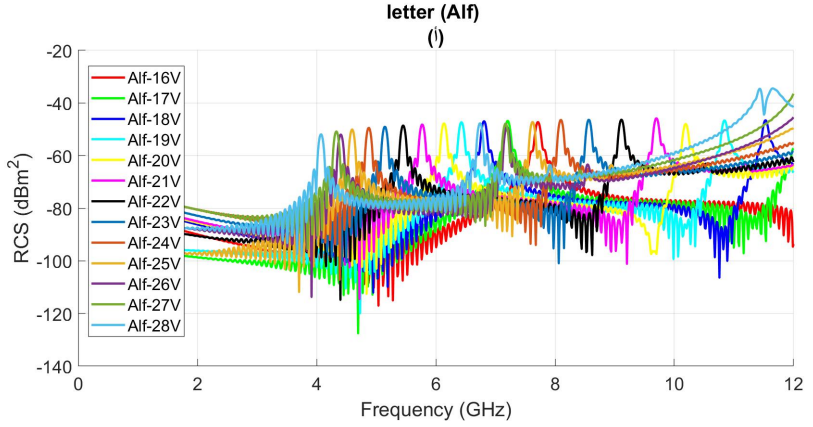

Figure 7: Cross polar RCS results of letter tag Alf (أ) for Calibri font type in different sizes

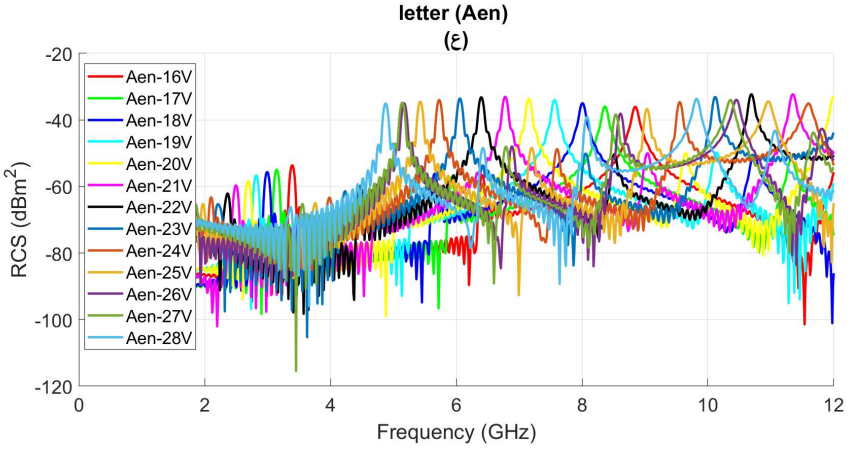

Figure 8: Cross polar RCS Results of letter tag Aen (ع) for Arial font type in different sizes

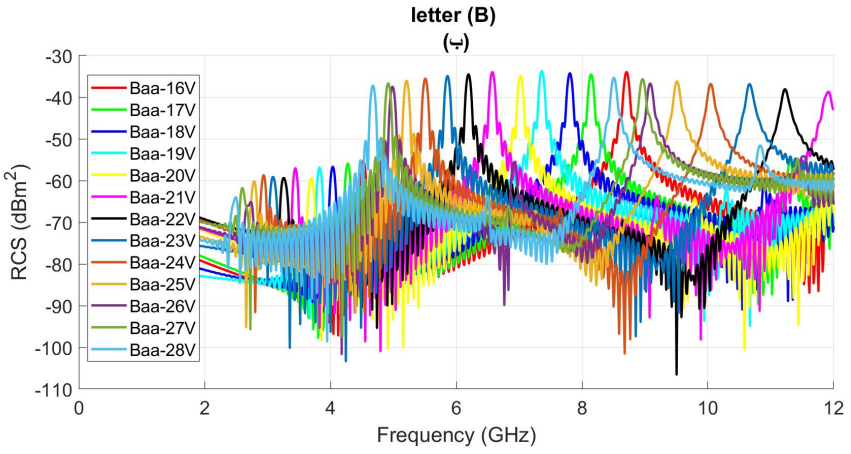

Figure 9: Cross polar RCS Results of letter tag Baa (ب) for Arial font type in different sizes

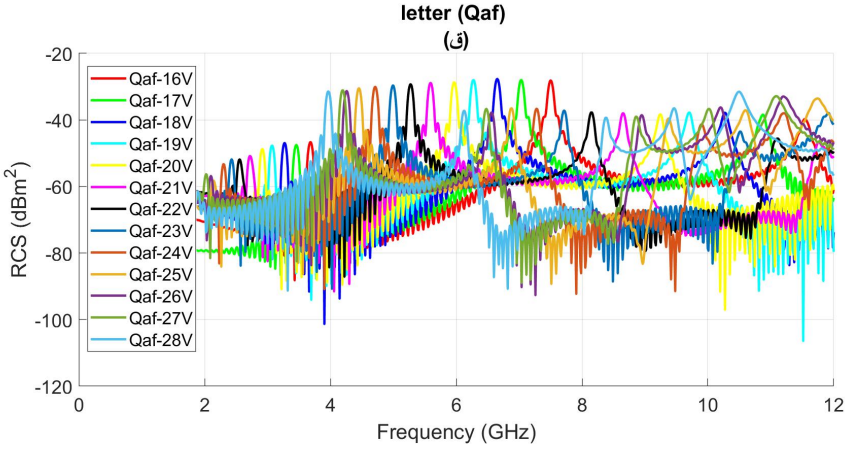

Figure 10: Cross polar RCS results of letter tag (ق) for Times New Roman font type in different font sizes

with all 13 analyzed sizes. The impact of changing the font size of letter tag Baa (ب) on its signature EMS with same Arial font type is illustrated in Figure 9. Figure 10 presents the same impact for letter tag Qaf (ق) for the Times New Roman font .

From Figures 6, 7, 8, 9, and 10, one can conclude the following observations on the effect of changing the font size on the RCS results: - The resonances shift up towards higher frequencies with the decrease in the tag's size. This observation is applicable for all font types despite each font type has its own unique RCS. - The relationship between resonance frequencies and font size is proportional. When the font size increases, the number of unique resonance frequencies increases for that particular letter tag in the analyzed frequency range, irrespective of the font type .

2.3. Effects of Changing the Font Type

This sections details the impact of the variation in the font type on the obtained RCS responses of the analyzed Arabic alphabet tags. It is evident that for a fixed font size, the change of the font type will have an impact on the back-scattered RCS characteristics of the Arabic letter tags. This can be noticed by comparing the vertical polarization RCS curves shown in Figure 6 to those shown in Figure 7 for any fixed font size. The change in font type from Arial to Calibri for letter tag Alf (أ) brings noticeable variations in its observed RCS response for any fixed font size.

As pointed earlier, three font types are considered in this study: Arial, Calibri, and Times New Roman (TNR). Each font type has its specific geometrical shape and structure that makes each resultant designed letter tag unique, and thus it will have a different RCS result. This has been demonstrated by comparing the cross polar RCS results of أ-tag for all three font types in Figure 11 for three font sizes namely, 17 mm, 21 mm, and 25 mm, respectively . The RCS analysis of all tags were performed for all 13 sizes with three font types. However, only limited font sizes results are reported here for brevity and clear comparison. In Figure 11, the dominate resonance peaks are noticed at 7.589 GHz (Arial), 7.204 GHz (Calibri), and 7.105 GHz (TNR) for analyzed أ-tag of firm 17 mm size. As shown in the figure, the change of the size to 21 mm has brought new distinct resonance at 6.181 GHz for Arial, two new resonances for Calibri, at , 5.774 GHz and 9.701 GHz, and two other for Times New Roman at 5.763 GHz and 11.2 GHz for the same tag . Similarly, the variations in the curve properties for tag size of 25 mm can be observed in Figure 11. This comparison reflects that the current distribution on the metallic tag structure varies with the change in its geometrical properties. This produces different RCS responses for the same tag of different font types. The variations in the resonances data occurs because every font type has a particular geometric shape with specific parameters, which will vary the induced current distribution on the tag's surface .

Figure 12 shows how the Baa (ب) tag shape is changing from one font type to another using three font sizes. Figure 13 shows the RCS results of tag ب in Arial, Calibri, and TNR for the illustrated tag shapes in Figure 12. When

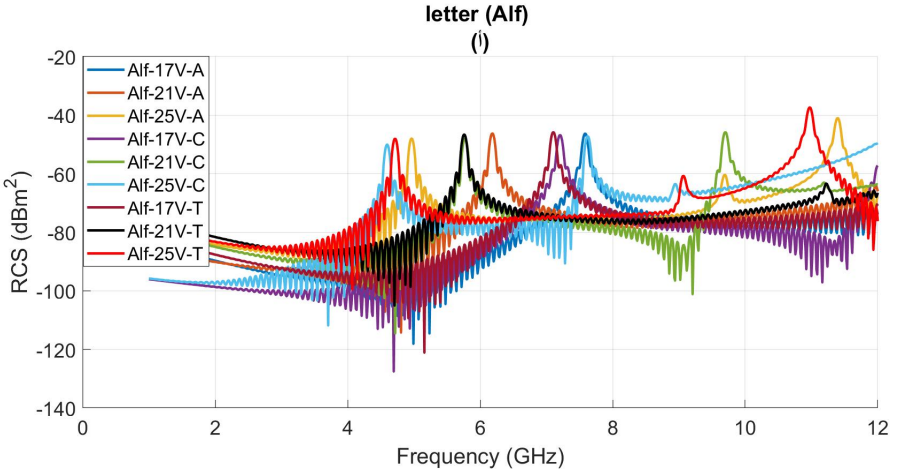

Figure 11: Cross polar RCS Results of letter tag Alf (أ) for Arial, Calibri, and Times New Roman font types of sizes 17 mm, 21 mm, and 25 mm

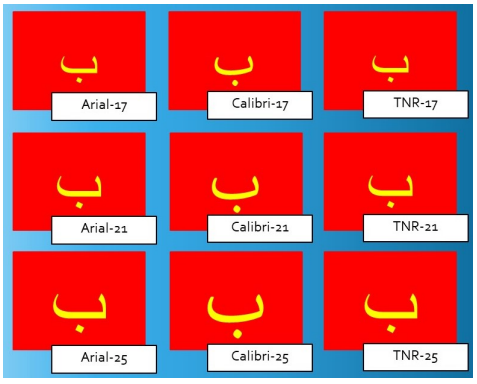

Figure 12: Baa (ب) tags in Arial, Calibri and Times New Roman font type with font sizes of 17 mm, 21 mm, and 25 mm

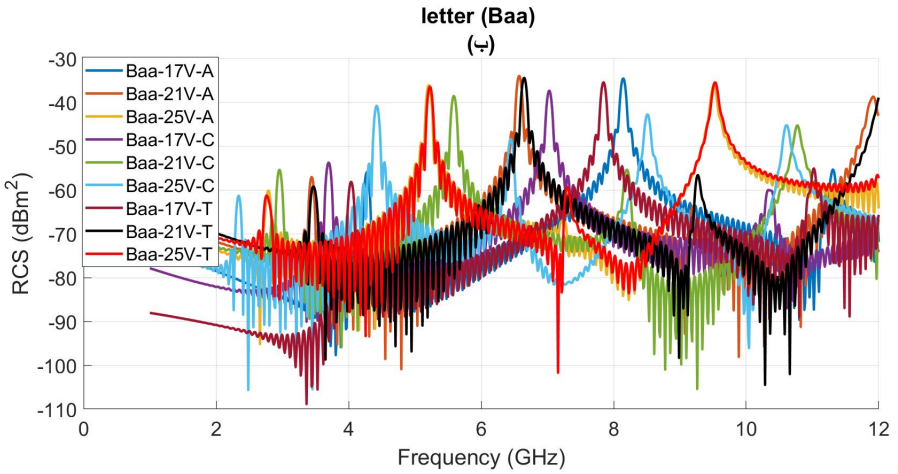

Figure 13: Cross polar RCS Results of letter tag Baa (ب) for Arial, Calibri, and Times New Roman font type of sizes 17 mm, 21 mm, and 25 mm

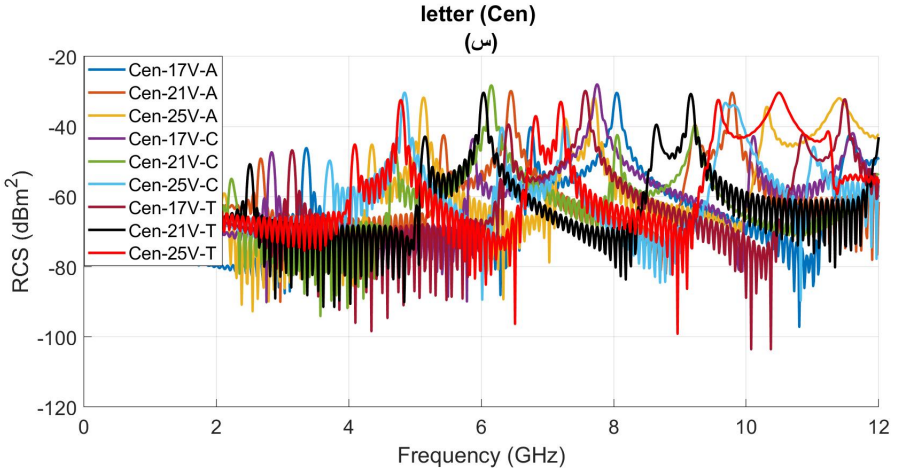

Figure 14: Cross polar RCS Results of letter Cen (س) for Arial, Calibri, and Times New Roman font types of sizes 17 mm, 21 mm, and 25 mm

we compared the Arial tag versus the Calibri tag, we noticed a considerable decrease in resonance frequency and more resonance peaks for Calibri tags. However , when the Arial is compared to the TNR , the decrease in resonance frequency is tiny. This is because the difference in tag structure is less for the Ariel and TNR tags as compared to Calibri tags. The same effect will apply to all other font types for all other alphabet tags. This can be deduced from the illustrated results of alphabets س and ل in Figures 14 and 15, respectively. The procedure is repeated with all tags in all font types while varying the font size and the resulting RCS results are accordingly recorded.

It is clear from the comparison of Figures 6 - 11, and 13 - 15 that the resonance characteristics of the realized tags are highly sensitive to any change in the letter tag's font type and size . This also indicates the reconfigurable nature of the designed Arabic letter tags. The conventional approaches of using look-up tables and frequency shift analysis are not useful here for the detection of the tags. This stems from the fact that, as elaborated thus far, the frequency shift has variable characteristics for each different Arabic letter tag. This makes the conventional approaches clumsy and inefficient. The proposed solution framework provides a robust and and efficient solution to this problem which is discussed in the next section.

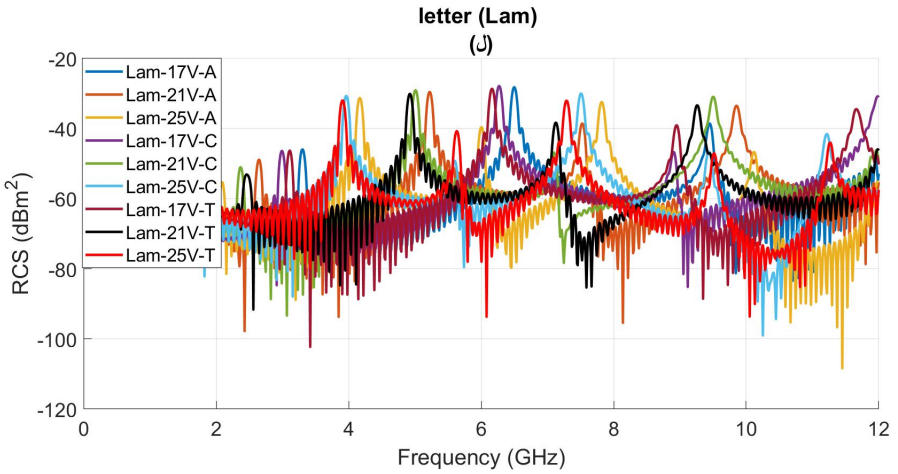

Figure 15: Cross polar RCS Results of letter Lam (ل) for Arial, Calibri, and Times New Roman font types of sizes 17 mm, 21 mm, and 25 mm

3. DL-based Classification Framework

Figure 16 shows the proposed deep learning system framework in detail. The proposed deep learning model consists of 4 stages that will classify letters RCS responses into Arabic alphabet names. The first stage is the data input/data generation stage to get the co- and cross-polar RCS of each tag with three different font types and 18 sizes as discussed in Section 2. The dataset for this study constitutes of horizontal and vertical RCS results of 28 Arabic alphabet letters for three font types, each with 13 font sizes. The generated combined data of size [28 (letters) x 13 (font sizes) x 1001

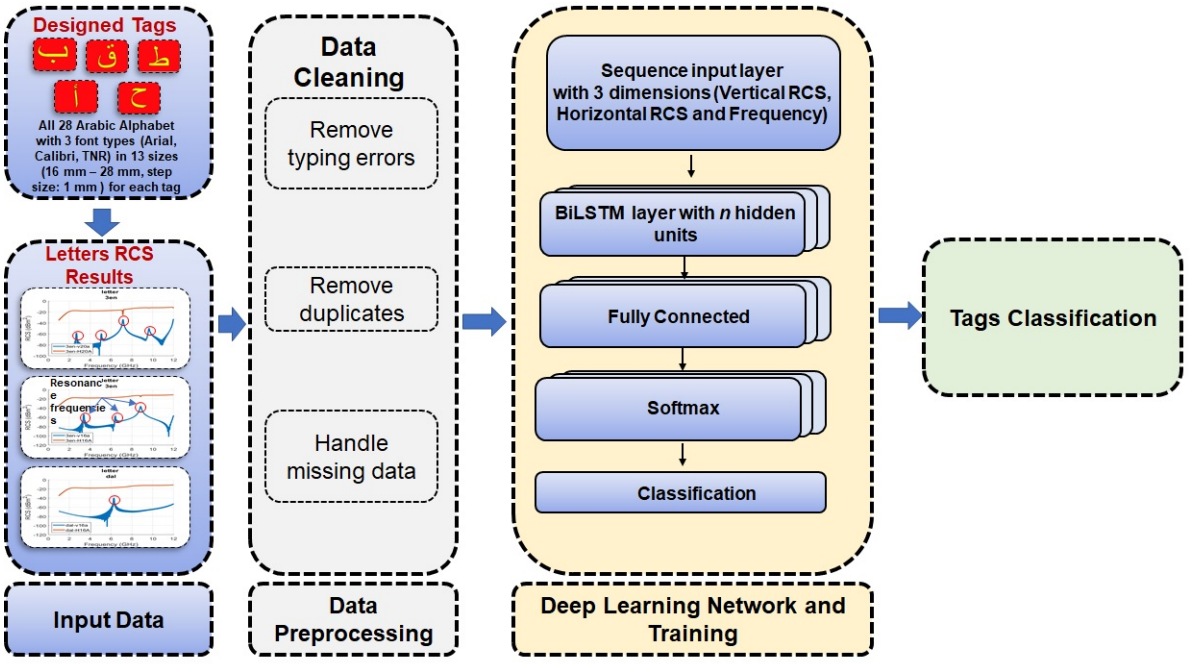

Figure 16: Proposed deep learning-based system framework for the robust detection and classification of chipless Arabic letters (the n represents hidden unit of BiLSTM network with tested values of 100/125/150 for this study)

Figure 17: Design of a simple LSTM network for classification

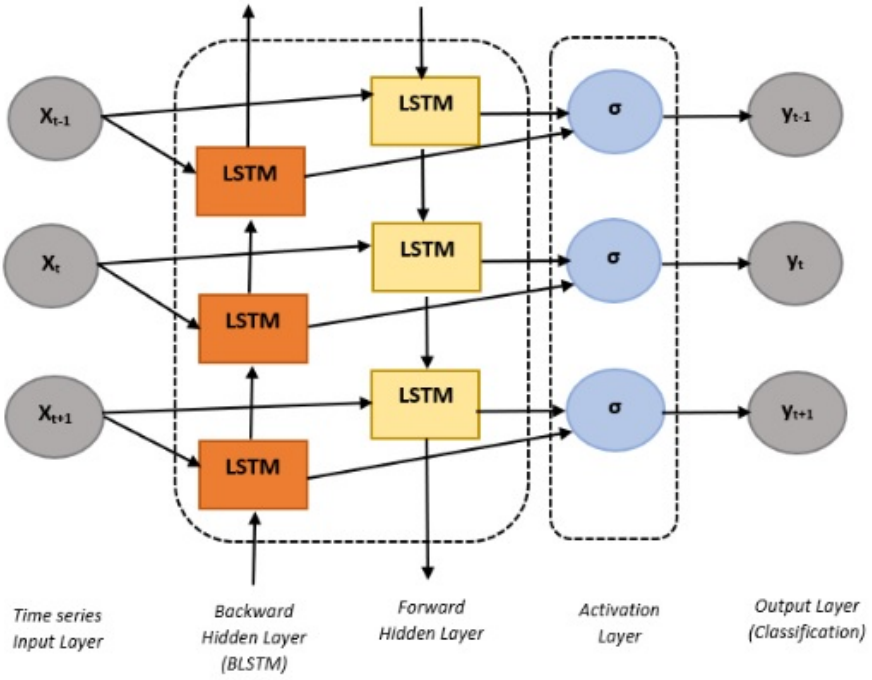

Figure 18: Architecture of a simple BiLSTM network

(frequency steps) x 2 (polarizations)] x 3 (font types) is then imported to MATLAB software as the input of the second stage, which is the pre-processing stage of the proposed framework.

In the second stage of data pre-processing, data cleaning and formatting is performed to convert all the data in one form. This includes removing typing errors in tags names, removing duplicates, and handling the missing data.

Finally, in the network training stage, the data is input to the deep learning Bidirectional-Long short-term memory (BiLSTM) network. Choosing a classification model from classical machine learning algorithms such as SVM, knearest neighbors (KNN), and decision trees or deep learning algorithms such as BiLSTM, depends on several factors such as the data type, dataset size, and the number of classes. The BiLSTM network is chosen in this study as this is a multi-class classification problem of 28 classes represented by the 28 Arabic alphabets tags of various font types and font sizes. Furthermore, the BiLSTM is better when using sequential or time-series data similar to our dataset as it can learn long term dependencies [33].

LSTM is a deep learning artificial recurrent neural network (RNN) architecture. Unlike traditional feed-forward neural networks, LSTM has feedback connections that enable it to process both single and complex data sequences [34, 35]. Figure 17 shows the design of a simple LSTM network for the classification problem. The main components of an LSTM network are a sequence input layer and an LSTM layer. The details about the architecture of BiLSTM are presented in Figure 18. BiLSTM is just putting two LSTMs together. The main principle behind bidirectional recurrent neural networks (BRNN) is to present each training sequence forwards and backward to two independent recurrent networks. The output layer will receive the sequence from both directions, which means that at any point

in a particular sequence, the BRNN possesses complete, sequential knowledge about all points before and after as explained in Figure 18. Bidirection runs the inputs from past to future and from future to past.

In our proposed framework, the BiLSTM architecture employs Convolutional Neural Network (CNN) layers for feature extraction to perform data regression or classification. As illustrated in Figure 17 and 18, a sequence input layer feeds data into the network in a sequence or a time series format. The network progresses to an LSTM layer. Finally, the network concludes with a fully connected layer, a softmax layer, and a classification output layer to forecast class labels.

The employed BiLSTM network for this study data has n hidden units with tested values of 100/125/150 and three input layers. This will generate the classification results as depicted in stage four of Figure 16. The details about the experimental results based on proposed deep learning framework are presented in next section.

4. Experimental Classification Results

This study dataset contains the RCS results of 28 Arabic alphabets in two different polarizations (Horizontal, Vertical), with three different font types (Arial, Times New Roman, Calibri) and 13 font sizes (16 - 28 mm with a step size of 1 mm). Figure 19 explains the distribution of dataset for the different experiments. It makes the total dataset to be [28 (letters) x 13 (font sizes) x 1001 (frequency steps) x 2 (polarizations)] x 3 (font types). The generated tags RCS data is examined very well with all major combinations of input data and network settings. Multi class classification of all realised 28 Arabic alphabet tags of various font types and sizes makes the problem challenging.

We performed the hyper-parameter optimization and ablation study of the proposed BiLSTM model by designing different experiments (see Figure 19) to analyze the impact of variations in the input data characteristics as well as network parameters such as input size, hidden units, max Epochs, learning rate, and cross-validation technique etc.

4.1. Impact on RCS Data Polarization on Network Performance

It is observed from the presented analysis in Section 2 that accurate identification of each letter tag depends on the its back scattered EM characteristics (RCS) in both horizontal and vertical polarizations. Therefore, firstly, the impact the change in the input data with respect to the polarization (horizontal, vertical, and combined) for a fixed font type with all 13 font sizes on the network performance is analyzed. The major BiLSTM network settings are fixed to input size of 2, maximum hidden units of 100, maxEpochs of 600, and a learning rate of 0.001. This network setting is used as a benchmark for all onward conducted experiments.

Each font type data is used separately to train the proposed network to detect the tag labels. We started with Times New Roman (TNR) tags data of all 28 tags with 13 sizes of each. The generated RCS data is tested in three different

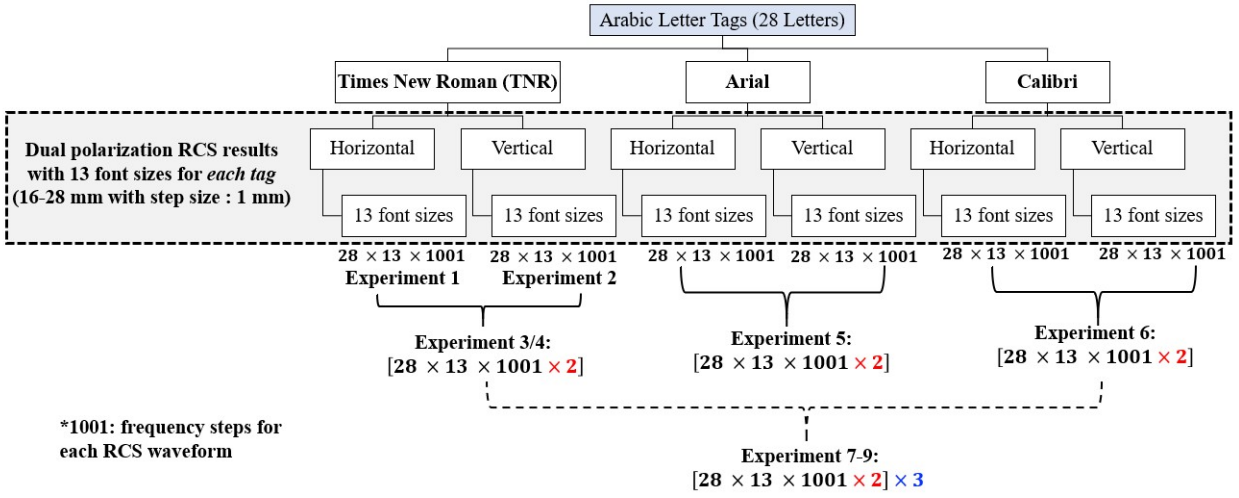

Figure 19: Dataset details for the designed experiments

Table 3
Summary of all the experiments on Arial , Calibri and Times New Roman font types with different network learning rate and validation (k-fold and Leave-One-Out Cross-Validation (LOOCV) settings.

Exp	Data used for Experiments	BiLSTM Network	Network settings		
			Learning rate	k-fold	LOOCV
1	Times New Roman Font Type with Horizontal RCS results only	input size 2, hidden units 100 ,maxEpochs 600	0.001	No	No
2	Times New Roman Font Type with Vertical RCS results only	input size 2, hidden units 100 ,maxEpochs 600	0.001	No	No
3	Times New Roman Font Type of all sizes with Horizontal and Vertical RCS results	input size 3, hidden units 100 ,maxEpochs 600	0.001	No	No
4	Times New Roman Font Type of all sizes with Horizontal and Vertical RCS results	input size 3, hidden units 100 ,maxEpochs 600	0.001/0.01	No	No
5	Times New Roman Font Type of all sizes with Horizontal and Vertical RCS results	input size 3, hidden units 100/150 ,maxEpochs 600/1000	0.001	Yes	No
6	Arial Font Type of all sizes with Horizontal and Vertical RCS results	input size 3, hidden units 100/150 ,maxEpochs 600/1000	0.001	Yes	No
7	Calibri Font Type of all sizes with Horizontal and Vertical RCS results	input size 3, hidden units 100/150 ,maxEpochs 600/1000	0.001	Yes	No
8	All Font Types of all sizes with Horizontal and Vertical RCS results	input size 3, hidden units 125 ,maxEpochs 1000/1200	0.001	Yes	No
9	All Font Types of all sizes with Horizontal and Vertical RCS results	input size 3, hidden units 125 ,maxEpochs 1000/1200	0.001	No	Yes

configurations to analyze the impact of (1) only horizontal RCS results (Experiment 1); (2) only vertical RCS results (Experiment 2); and (3) combined horizontal and vertical RCS results (Experiment 3) on the model classification accuracy under the benchmark settings. Table 3 summarizes the input data and network characteristics for the all major experiments of this study. The complexity of the input data and network settings is increased in each succeeding experiment to analyze the impact of these variations on the perform acne of designed classification system.

In the first experiment of this category, only horizontal RCS results of 28 TNR font type tags with 13 sizes are used. This makes the input data size to be $28 \times 13 \times 1001$ as depicted in Figure 19. Here '1001' represents the frequency steps for each RCS waveform. In the second experiment , the input data is changed to only vertical RCS results ($28 \times 13 \times 1001$) with the same network settings of the first experiment. The combination of co- and cross polar RCS results (both polarizations) ($28 \times 13 \times 1001 \times 2$) is used as the input in the designed experiment 3 as illustrated in Figure 19.

The maximum achieved test accuracies of experiment 1 and experiment 2 are 29% and 64% ,respectively. Experiment 2 test accuracy is better than experiment 1 because the resonances in vertical RCS results have on-average more than 10 dB difference between resonances. This enhances the performance of the classification network when compared to the only horizontal RCS data (experiment 1). The best test accuracy result of 75% is obtained without any cross-validation when both horizontal and vertical RCS waveforms data is used as an input for the designed classification system in experiment 3. This same settings of the input data (combined co- and cross-polar results) is used for onward analyzed cases.

4.2. Impact of Learning Rate on Network Performance

Next, we examined the impact of the BiLSTM network learning rate on the training and test accuracy with no change in input data ($28 \times 13 \times 1001 \times 2$) and network settings as for experiment 3 (input size 3, hidden units 100, and maxEpochs 60). This is analyzed for two different learning rates of 0.01 and 0.001, respectively, and is termed as experiment 4 as illustrated in Table 3. The test accuracy dropped to 71% from 75% with the increase in the network learning rate to 0.01 from 0.001. The comparison of first four experiments reveals that the 100 hidden units of BiLSTM layer with network learning rate of 0.001 is an optimal choice for the analyzed classification network based on only TNR data

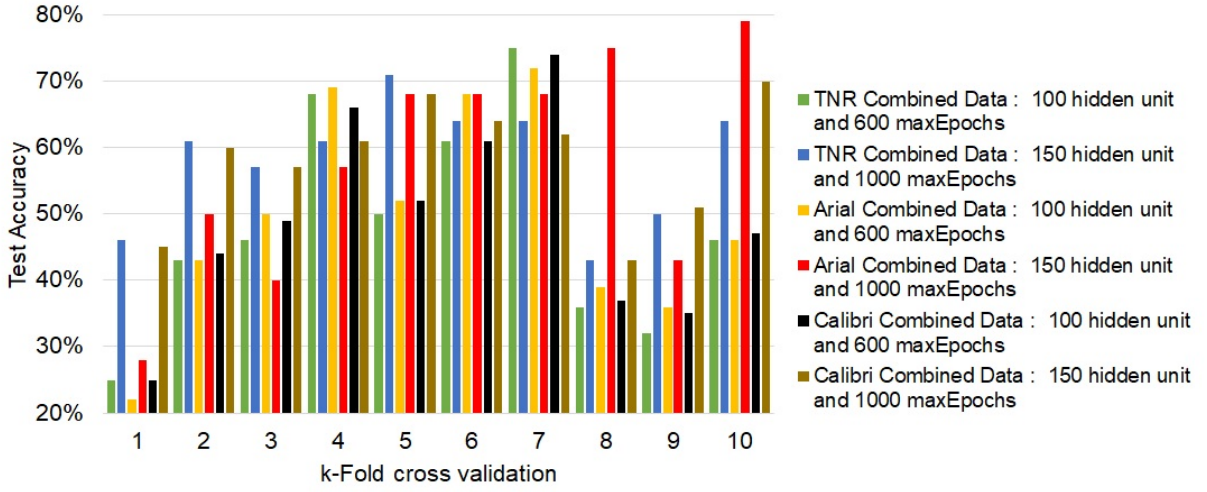

Figure 20: Comparison of test accuracies when utilizing k-fold cross-validation with different network settings for each separate font type data

4.3. Impact of Change in Tags Font Type on Network Performance with Cross-Validation

The next experiments (5-7) are designed for the building of a robust and generalized model that works well with all different tag types irrespective of their font type and size. The font type of the combined input data of all sizes is varied from TNR (Exp. 5) to Arial (Exp. 6) and to Calibri (Exp. 7) as illustrated in Figure 19. The size of data set for these experiments is $28 \times 13 \times 1001 \times 2$.

To minimize the impact of over-fitting for the robust design of the classifier, the k-fold cross-validation technique is used. As outlined in Table 3 besides employed k-fold cross-validation, BiLSTM network settings in terms of hidden units(100/150) and maxEpochs (600/1000) are also varied to analyze their impact on the network accuracy for further tuning of network with cross-validation impact.

Figure 20 shows the variations in the test accuracies of the network for the aforementioned settings of the network for only TNR, Arial, and Calibri data as separate inputs of the network. We noticed that the variations in both BiLSTM layer settings and k-fold cross-validation level have significant impact on the classification accuracy of the network. As the input RCS data characteristics are varying with the change in font type (see Figures 6 - 11, and 13 - 15), it even impacts the network performance for a fixed BiLSTM layer settings and k-fold cross-validation. It can be observed from Figure 20 that the network performance improves in terms of test accuracy with the increase of the folding rate in the employed cross-validation technique. Overall higher test accuracy for the TNR and Calibri data is noted for the 4- to 7-fold cross-validations. The test accuracy of the DL detection network is 50% for TNR data, and 52% for both Arial and Calibri data for 100 hidden units of BiLSTM layer and resampling using 5-fold cross.-validation. These number changes to 71% for TNR data, and 68% for both Arial and Calibri data when the hidden units of BiLSTM layer are increased to 150 with same 5-fold cross-validation.

The highest test accuracy of 75% and 74% is recorded with a 7-fold cross-validation and 100 hidden units of the BiLSTM layer for the TNR and Calibri data, respectively. However, the Arial data shows a maximum accuracy of 79% when data resampling is done using a 10-fold cross-validation with 150 hidden units and 1000 maxEpoches of the BiLSTM network. These maximum accuracies are observed under different network settings (see Figure 20). The change in font type of Arabic letter tags modifies the multidimensional detection and identification problem, since totally different resonance dips are recorded for each letter tag as illustrated in Section 2. This requires variations in network settings, as well as the folding rate in the k-fold cross-validation to get the highest possible test accuracy for different classes of input data.

4.4. Impact of Combined Data on Network Performance with Cross-Validation

The previous experiments utilized each font type with all sizes belonging to it. Next, we combine all font sizes and types to test the whole data set as illustrated in Figure 19. This experiment (Exp. 8) dataset consists of horizontal and vertical RCS results of three font types and all 13 font sizes per font type. Thus the total size of the input data becomes

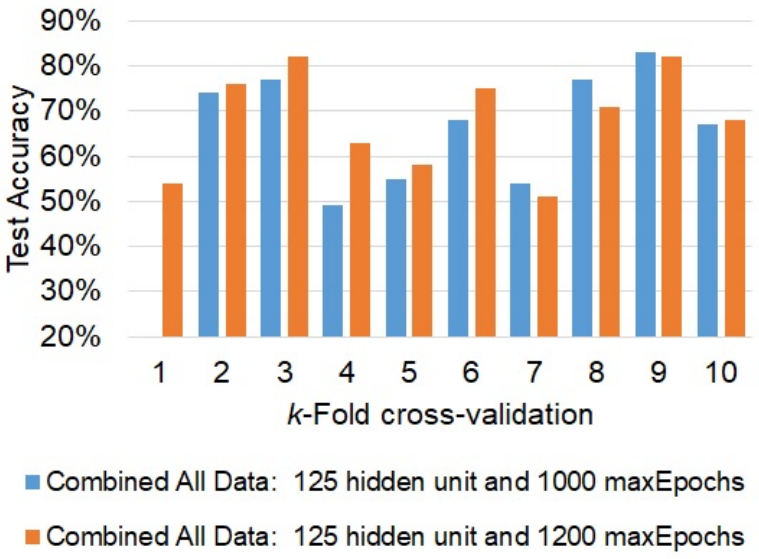

Figure 21: Comparison of test accuracies when utilizing k-fold cross-validation with different network settings for combined all font types and sizes data

$[(28 \times 13 \times 1001 \times 2)] \times 3$. The combination of data ensures that the system will classify Arabic RFID tags based on the information given on any letter tag with any of the three font types and 13 font sizes. This evaluation will give a good indication about the ability of the system to detect Arabic alphabet tags irrespective of the trained or new data samples.

First, the analysis of this mixed dataset of all font types and sizes is performed using k-fold cross-validation, which is referred to as experiment 8. Again we repeated this experiment using different settings of the BiLSTM layers in terms of the variations in hidden units and number of maxEpochs. The objective was to obtain optimal network settings that ensure the highest test accuracy. The comparison of the obtained test accuracies for the two optimal network settings *i.e.* hidden units of 150 and maxEpochs of 1000/1200, is shown in Figure 21. The network was also tested under various other network settings, but only major results are reported here for brevity.

We can notice from Figure 21 that mixing of the all font types and sizes as input of the proposed DL system enhances its overall classification accuracies when compared with the earlier results of separate font types data (Experiments 5-7). For these experiments, the highest test accuracy of 83% was recorded in 9th fold. This was obtained with 125 hidden units of the BiLSTM layer and a maximum limitation of 1000 epochs. The increase of maxEpochs to 1200 further increases the testing time and computational cost of the network but did not bring a significant improvement to the accuracy level as compared to same network settings with maximum epochs of 1000. Figure 22 presents the confusion matrix for the best performance obtained in classifying Arabic letter tags of different fonts and sizes using a 10-fold cross-validation.

Lastly, the network validation setting was changed to Leave-One-Out Cross-Validation (LOOCV), and experiment 9 is repeated with this setting to find an optimal solution. LOOCV is referred as the logical extreme of k-Fold cross validation where k becomes the total number of data points (N) in the analyzed dataset. Figure 23 compares the network performance for the two optimized network settings. The classification accuracy varies with the change in the number of iterations of LOOCV for both network settings. The iteration 12 produces a superior accuracy of 89% when the network is trained with 125 hidden units of BiLSTM layer and maxEpochs of 1200. The reduction of maxEepochs to 1000 makes the classification system relatively computational inexpensive with on-average 2-3% reduction in the classification accuracy as illustrated in Figure 23. The comparison of Figures 21 and 23 reflects that LOOCV validation outperforms the k-fold cross-validation. The confusion matrix for this overall best performance of the realized classification network of Arabic letter tags is shown in Figure 24. This network can classify the 28 Arabic letter tags of any font type from Arial, TNR, and Calibri with any size from 16 mm to 28 mm with 89% accuracy.

	Aen	Taa	Haa	Gaf	Alf	Baa	Cen	Dad	Dal	Faa	Gem	Ghen	Haa	Kaf	Kha	Lam	Mem	Noon	Raa	Saad	Shen	Taa	Thaa	Waw	Yaa	Zal	Zen	Zza	
Aen	1 3.6%	0 0.0%	0 0.0%	0 0.0%	0 0.0%	0 0.0%	0 0.0%	0 0.0%	0 0.0%	0 0.0%	0 0.0%	1 3.6%	0 0.0%	0 0.0%	0 0.0%	0 0.0%	0 0.0%	0 0.0%	0 0.0%	0 0.0%	0 0.0%	0 0.0%	0 0.0%	0 0.0%	0 0.0%	0 0.0%	0 0.0%	0 0.0%	50% 50%
Taa	0 0.0%	1 3.6%	0 0.0%	0 0.0%	0 0.0%	0 0.0%	0 0.0%	0 0.0%	0 0.0%	0 0.0%	0 0.0%	0 0.0%	0 0.0%	0 0.0%	0 0.0%	0 0.0%	0 0.0%	0 0.0%	1 3.6%	0 0.0%	0 0.0%	0 0.0%	0 0.0%	0 0.0%	0 0.0%	0 0.0%	0 0.0%	0 0.0%	50% 50%
Haa	0 0.0%	0 0.0%	1 3.6%	0 0.0%	0 0.0%	0 0.0%	0 0.0%	0 0.0%	0 0.0%	0 0.0%	0 0.0%	0 0.0%	0 0.0%	0 0.0%	0 0.0%	0 0.0%	0 0.0%	0 0.0%	0 0.0%	0 0.0%	0 0.0%	0 0.0%	0 0.0%	1 3.6%	0 0.0%	0 0.0%	0 0.0%	0 0.0%	50% 50%
Gaf	0 0.0%	0 0.0%	0 0.0%	0 0.0%	0 0.0%	0 0.0%	0 0.0%	0 0.0%	0 0.0%	0 0.0%	0 0.0%	0 0.0%	0 0.0%	0 0.0%	0 0.0%	0 0.0%	0 0.0%	0 0.0%	0 0.0%	0 0.0%	0 0.0%	0 0.0%	0 0.0%	0 0.0%	0 0.0%	0 0.0%	0 0.0%	0 0.0%	NaN% NaN%
Alf	0 0.0%	0 0.0%	0 0.0%	0 0.0%	1 3.6%	0 0.0%	0 0.0%	0 0.0%	0 0.0%	0 0.0%	0 0.0%	0 0.0%	0 0.0%	0 0.0%	0 0.0%	0 0.0%	0 0.0%	0 0.0%	0 0.0%	0 0.0%	0 0.0%	0 0.0%	0 0.0%	0 0.0%	0 0.0%	0 0.0%	0 0.0%	0 0.0%	50% 50%
Baa	0 0.0%	0 0.0%	0 0.0%	0 0.0%	0 0.0%	1 3.6%	0 0.0%	0 0.0%	0 0.0%	0 0.0%	0 0.0%	0 0.0%	0 0.0%	0 0.0%	0 0.0%	0 0.0%	0 0.0%	0 0.0%	0 0.0%	0 0.0%	0 0.0%	0 0.0%	0 0.0%	0 0.0%	0 0.0%	0 0.0%	0 0.0%	0 0.0%	100% 0.0%
Cen	0 0.0%	0 0.0%	0 0.0%	0 0.0%	0 0.0%	0 0.0%	1 3.6%	0 0.0%	0 0.0%	0 0.0%	0 0.0%	0 0.0%	0 0.0%	0 0.0%	0 0.0%	0 0.0%	0 0.0%	0 0.0%	0 0.0%	0 0.0%	0 0.0%	0 0.0%	0 0.0%	0 0.0%	0 0.0%	0 0.0%	0 0.0%	0 0.0%	100% 0.0%
Dad	0 0.0%	0 0.0%	0 0.0%	0 0.0%	0 0.0%	0 0.0%	0 0.0%	1 3.6%	0 0.0%	0 0.0%	0 0.0%	0 0.0%	0 0.0%	0 0.0%	0 0.0%	0 0.0%	0 0.0%	0 0.0%	0 0.0%	0 0.0%	0 0.0%	0 0.0%	0 0.0%	0 0.0%	0 0.0%	0 0.0%	0 0.0%	0 0.0%	100% 0.0%
Dal	0 0.0%	0 0.0%	0 0.0%	0 0.0%	0 0.0%	0 0.0%	0 0.0%	0 0.0%	1 3.6%	0 0.0%	0 0.0%	0 0.0%	0 0.0%	0 0.0%	0 0.0%	0 0.0%	0 0.0%	0 0.0%	0 0.0%	0 0.0%	0 0.0%	0 0.0%	0 0.0%	0 0.0%	0 0.0%	0 0.0%	0 0.0%	0 0.0%	100% 0.0%
Faa	0 0.0%	0 0.0%	0 0.0%	0 0.0%	0 0.0%	0 0.0%	0 0.0%	0 0.0%	0 0.0%	1 3.6%	0 0.0%	0 0.0%	0 0.0%	0 0.0%	0 0.0%	0 0.0%	0 0.0%	0 0.0%	0 0.0%	0 0.0%	0 0.0%	0 0.0%	0 0.0%	0 0.0%	0 0.0%	0 0.0%	0 0.0%	0 0.0%	100% 0.0%
Gem	0 0.0%	0 0.0%	0 0.0%	0 0.0%	0 0.0%	0 0.0%	0 0.0%	0 0.0%	0 0.0%	0 0.0%	1 3.6%	0 0.0%	0 0.0%	0 0.0%	0 0.0%	0 0.0%	0 0.0%	0 0.0%	0 0.0%	0 0.0%	0 0.0%	0 0.0%	0 0.0%	0 0.0%	0 0.0%	0 0.0%	0 0.0%	0 0.0%	100% 0.0%
Ghen	0 0.0%	0 0.0%	0 0.0%	0 0.0%	0 0.0%	0 0.0%	0 0.0%	0 0.0%	0 0.0%	0 0.0%	0 0.0%	1 3.6%	0 0.0%	0 0.0%	0 0.0%	0 0.0%	0 0.0%	0 0.0%	0 0.0%	0 0.0%	0 0.0%	0 0.0%	0 0.0%	0 0.0%	0 0.0%	0 0.0%	0 0.0%	0 0.0%	100% 0.0%
Haa	0 0.0%	0 0.0%	0 0.0%	0 0.0%	0 0.0%	0 0.0%	0 0.0%	0 0.0%	0 0.0%	0 0.0%	0 0.0%	0 0.0%	1 3.6%	0 0.0%	0 0.0%	0 0.0%	0 0.0%	0 0.0%	0 0.0%	0 0.0%	0 0.0%	0 0.0%	0 0.0%	0 0.0%	0 0.0%	0 0.0%	0 0.0%	0 0.0%	100% 0.0%
Kaf	0 0.0%	0 0.0%	0 0.0%	0 0.0%	0 0.0%	0 0.0%	0 0.0%	0 0.0%	0 0.0%	0 0.0%	0 0.0%	0 0.0%	0 0.0%	1 3.6%	0 0.0%	0 0.0%	0 0.0%	0 0.0%	0 0.0%	0 0.0%	0 0.0%	0 0.0%	0 0.0%	0 0.0%	0 0.0%	0 0.0%	0 0.0%	0 0.0%	100% 0.0%
Kha	0 0.0%	0 0.0%	0 0.0%	0 0.0%	0 0.0%	0 0.0%	0 0.0%	0 0.0%	0 0.0%	0 0.0%	0 0.0%	0 0.0%	0 0.0%	0 0.0%	0 0.0%	0 0.0%	0 0.0%	0 0.0%	0 0.0%	0 0.0%	0 0.0%	0 0.0%	0 0.0%	0 0.0%	0 0.0%	0 0.0%	0 0.0%	0 0.0%	NaN% NaN%
Lam	0 0.0%	0 0.0%	0 0.0%	0 0.0%	0 0.0%	0 0.0%	0 0.0%	0 0.0%	0 0.0%	0 0.0%	0 0.0%	0 0.0%	0 0.0%	0 0.0%	0 0.0%	1 3.6%	0 0.0%	0 0.0%	0 0.0%	0 0.0%	0 0.0%	0 0.0%	0 0.0%	0 0.0%	0 0.0%	0 0.0%	0 0.0%	0 0.0%	100% 0.0%
Mem	0 0.0%	0 0.0%	0 0.0%	0 0.0%	0 0.0%	0 0.0%	0 0.0%	0 0.0%	0 0.0%	0 0.0%	0 0.0%	0 0.0%	0 0.0%	0 0.0%	0 0.0%	0 0.0%	1 3.6%	0 0.0%	0 0.0%	0 0.0%	0 0.0%	0 0.0%	0 0.0%	0 0.0%	0 0.0%	0 0.0%	0 0.0%	0 0.0%	100% 0.0%
Noon	0 0.0%	0 0.0%	0 0.0%	0 0.0%	0 0.0%	0 0.0%	0 0.0%	0 0.0%	0 0.0%	0 0.0%	0 0.0%	0 0.0%	0 0.0%	0 0.0%	0 0.0%	0 0.0%	0 0.0%	0 0.0%	0 0.0%	0 0.0%	0 0.0%	0 0.0%	1 3.6%	0 0.0%	0 0.0%	0 0.0%	0 0.0%	0 0.0%	0.0% 100%
Raa	0 0.0%	0 0.0%	0 0.0%	0 0.0%	0 0.0%	0 0.0%	0 0.0%	0 0.0%	0 0.0%	0 0.0%	0 0.0%	0 0.0%	0 0.0%	0 0.0%	0 0.0%	0 0.0%	0 0.0%	0 0.0%	1 3.6%	0 0.0%	0 0.0%	0 0.0%	0 0.0%	0 0.0%	0 0.0%	0 0.0%	0 0.0%	0 0.0%	100% 0.0%
Saad	0 0.0%	0 0.0%	0 0.0%	0 0.0%	1 3.6%	0 0.0%	0 0.0%	0 0.0%	0 0.0%	0 0.0%	0 0.0%	0 0.0%	0 0.0%	0 0.0%	0 0.0%	0 0.0%	0 0.0%	0 0.0%	0 0.0%	0 0.0%	0 0.0%	0 0.0%	0 0.0%	0 0.0%	0 0.0%	0 0.0%	0 0.0%	0 0.0%	0.0% 100%
Shen	0 0.0%	0 0.0%	0 0.0%	0 0.0%	0 0.0%	0 0.0%	0 0.0%	0 0.0%	0 0.0%	0 0.0%	0 0.0%	0 0.0%	0 0.0%	0 0.0%	0 0.0%	0 0.0%	0 0.0%	0 0.0%	0 0.0%	0 0.0%	0 0.0%	0 0.0%	0 0.0%	0 0.0%	0 0.0%	0 0.0%	0 0.0%	0 0.0%	NaN% NaN%
Taa	0 0.0%	0 0.0%	0 0.0%	0 0.0%	0 0.0%	0 0.0%	0 0.0%	0 0.0%	0 0.0%	0 0.0%	0 0.0%	0 0.0%	0 0.0%	0 0.0%	0 0.0%	0 0.0%	0 0.0%	0 0.0%	0 0.0%	0 0.0%	0 0.0%	1 3.6%	0 0.0%	0 0.0%	0 0.0%	0 0.0%	0 0.0%	0 0.0%	100% 0.0%
Thaa	0 0.0%	0 0.0%	0 0.0%	0 0.0%	0 0.0%	0 0.0%	0 0.0%	0 0.0%	0 0.0%	0 0.0%	0 0.0%	0 0.0%	0 0.0%	0 0.0%	0 0.0%	0 0.0%	0 0.0%	0 0.0%	0 0.0%	0 0.0%	0 0.0%	1 3.6%	1 3.6%	0 0.0%	0 0.0%	0 0.0%	0 0.0%	0 0.0%	50% 50%
Waw	0 0.0%	0 0.0%	0 0.0%	0 0.0%	0 0.0%	0 0.0%	0 0.0%	0 0.0%	0 0.0%	0 0.0%	0 0.0%	0 0.0%	0 0.0%	0 0.0%	0 0.0%	0 0.0%	0 0.0%	0 0.0%	0 0.0%	0 0.0%	0 0.0%	0 0.0%	0 0.0%	1 3.6%	0 0.0%	0 0.0%	0 0.0%	0 0.0%	100% 0.0%
Yaa	0 0.0%	0 0.0%	0 0.0%	0 0.0%	0 0.0%	0 0.0%	0 0.0%	0 0.0%	0 0.0%	0 0.0%	0 0.0%	0 0.0%	0 0.0%	0 0.0%	0 0.0%	0 0.0%	0 0.0%	0 0.0%	0 0.0%	0 0.0%	0 0.0%	0 0.0%	0 0.0%	0 0.0%	1 3.6%	0 0.0%	0 0.0%	0 0.0%	100% 0.0%
Zal	0 0.0%	0 0.0%	0 0.0%	0 0.0%	0 0.0%	0 0.0%	0 0.0%	0 0.0%	0 0.0%	0 0.0%	0 0.0%	0 0.0%	0 0.0%	0 0.0%	0 0.0%	0 0.0%	0 0.0%	0 0.0%	0 0.0%	0 0.0%	0 0.0%	0 0.0%	0 0.0%	0 0.0%	0 0.0%	1 3.6%	0 0.0%	0 0.0%	100% 0.0%
Zen	0 0.0%	0 0.0%	0 0.0%	0 0.0%	0 0.0%	0 0.0%	0 0.0%	0 0.0%	0 0.0%	0 0.0%	0 0.0%	0 0.0%	0 0.0%	0 0.0%	0 0.0%	0 0.0%	0 0.0%	0 0.0%	0 0.0%	0 0.0%	0 0.0%	0 0.0%	0 0.0%	0 0.0%	0 0.0%	0 0.0%	1 3.6%	0 0.0%	100% 0.0%
Zza	0 0.0%	0 0.0%	0 0.0%	0 0.0%	0 0.0%	0 0.0%	0 0.0%	0 0.0%	0 0.0%	0 0.0%	0 0.0%	0 0.0%	0 0.0%	0 0.0%	0 0.0%	0 0.0%	0 0.0%	0 0.0%	0 0.0%	0 0.0%	0 0.0%	0 0.0%	0 0.0%	0 0.0%	0 0.0%	0 0.0%	0 0.0%	1 3.6%	100% 0.0%
	100% 0.0%	100% 0.0%	100% 0.0%	0.0% 100%	100% 0.0%	100% 0.0%	100% 0.0%	100% 0.0%	100% 0.0%	100% 0.0%	100% 0.0%	100% 0.0%	100% 0.0%	100% 0.0%	0.0% 100%	100% 0.0%	100% 0.0%	100% 0.0%	100% 0.0%	0.0% 100%	0.0% 100%	100% 0.0%	100% 0.0%	100% 0.0%	100% 0.0%	100% 0.0%	100% 0.0%	100% 0.0%	83% 17%

Figure 22: Confusion matrix for the best performance of classifying Arabic RFID tags using all font types and all font sizes using 10-Fold cross-validation

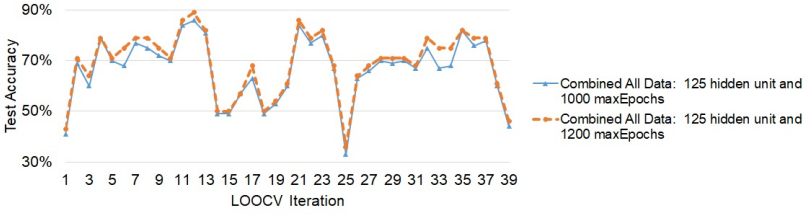

Figure 23: Comparison of test accuracies when utilizing LOOCV with different network settings for combined dataset

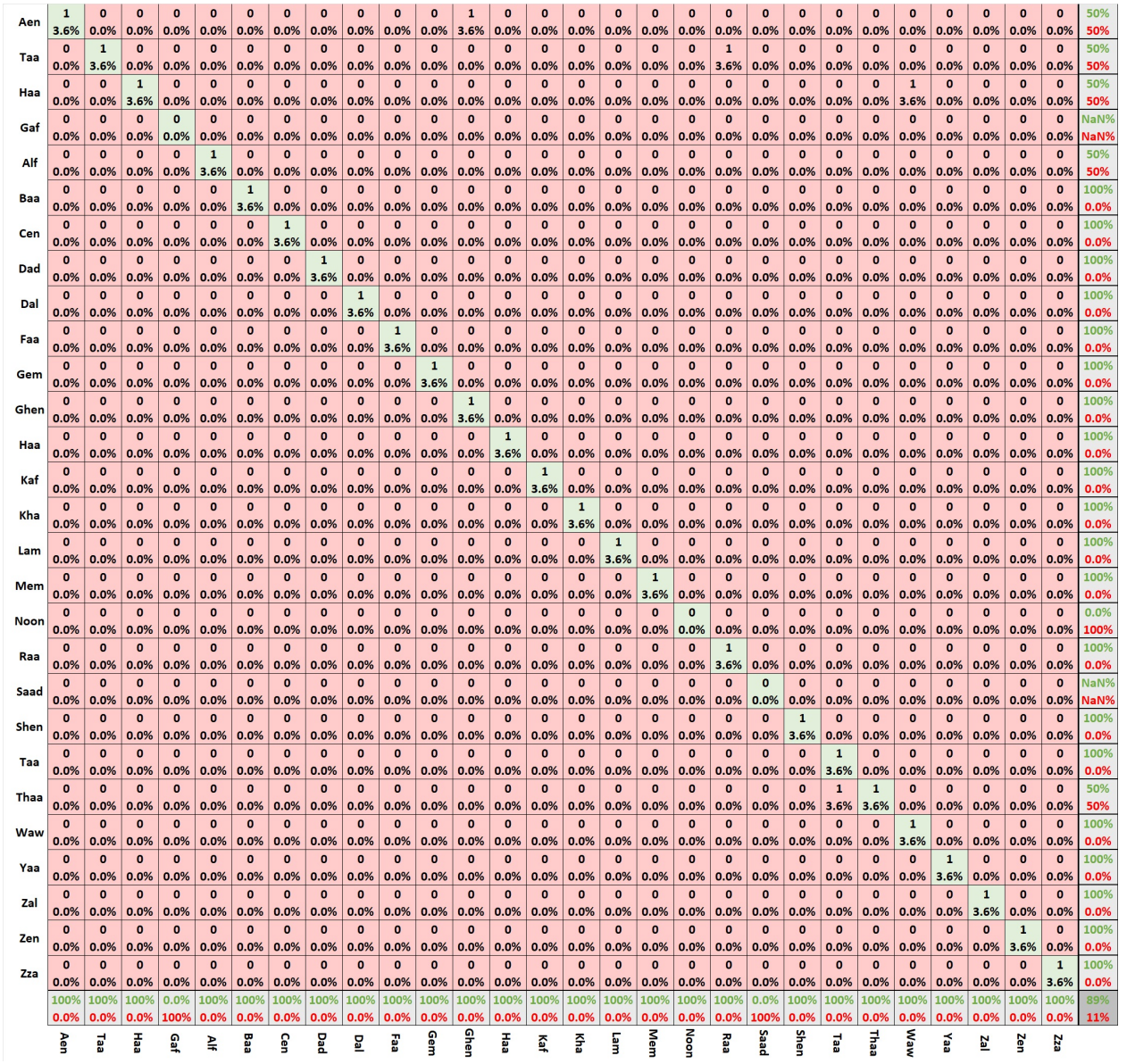

Figure 24: Confusion matrix for the best performance of classifying Arabic RFID tags using all font types and all font sizes using Leave-One-Out Cross-Validation (LOOCV)

The comparison of training and classification (test) accuracies for all conducted experiments is given in Table 4. It can be observed that the richness of the data increases both the training and the test accuracies as we moved to the data of Experiments 8 and 9. However, utilizing LOOCV makes the network computationally expensive compared to k-fold cross-validation.

5. Discussion and Analysis

The underlined classification problem of Arabic RFID tags of various fonts and sizes is considered a multiclass classification problem. The performance of the designed model will vary due to the mapping features (resonances) of the tags with different shapes and sizes in this multidimensional classification problem. The standard machine learning technique can be used with outstanding performance when dealing with binary classification problems but may not

Table 4
Comparison of training and test (classification) accuracies of Table 3 experiments

Experiment	Time Elapsed in Minutes	Training Accuracy	Test Accuracy
1	25	88.32%	29%
2	30	90.87%	64%
3	32	90.33%	75%
4	29	80.08%	65%
5	45	88.5%	70.5%
6	33	94.12%	75%
7	31	92.5%	74%
8	380	93.42%	83%
9	741	96.85%	89%

Table 5
Summary of performance analysis using different machine learning techniques with proposed Bi-LSTM network approach

Using *k*-Fold Cross Validation				
Data Set	**SVM**	**Tree**	**KNN**	**Proposed BiLSTM**
Time New Roman Only (Experiment-3)	3.40 %	14.40 %	12.60 %	- %
Arial Only (Experiment-6)	3.20 %	16.30 %	12.40 %	79 %
Calibri Only (Experiment-7)	2.60 %	14.60 %	9.50 %	70 %
Using *k*-Fold Cross Validation				
All Fonts Combined (Experiment-8)	6.40 %	17.30 %	27.40%	83%
Using LOOCV Cross Validation				
All Fonts Combined (Experiment-9)	6.20 %	16.30 %	26.80 %	89%

be useful when the number of classes (28) is high, as in this work. A comparison of the accuracies obtained using traditional machine learning techniques such as SVM, decision tree, and KNN with the proposed model is shown in Table 5. This comparison is made for the various experiments in Table 3. The classification accuracy for different experiments using these techniques is very low compared to the results achieved using the proposed Bi-LSTM network. This comparison reflects that the choice of the appropriate machine or deep learning classification algorithm is highly dependent on the characteristics of the data.

The analysis of the confusion matrices provides more insight into the characteristics (tags) that are poorly attributing to the achieved maximum 89% accuracy using all tags data. It can be seen from Figures 22 and 24 that there are some tags such as ب, ج, ظ , و which remains undetected and reduce the overall classification precision. The highest precision of 89% was obtained using LOOCV (experiment 9) for the confusion matrix of Figure 24. For further analysis, we removed these undetected tags from our dataset and repeated experiment 9 with same learning rate of 0.01. With the adjustment of the network hyper-parameters with different BiLSTM settings, we were able to achieve a classification accuracy of up to 96 % as illustrated in Figure 25.

Besides the analysis of the impact of some undetected tags on classification accuracy, we noticed from the confusion matrices of each font type alone (not shown here for brevity) in experiments 2, 3, and 7 that the size of tags too impact the achieved accuracy levels. The smaller size tags (*i.e.* size 16, 17, and 18) are detected with lower accuracy compared to the larger size tags (*i.e.* size 26, 27, and 28). It is because these smaller tags have fewer resonance peaks compared to larger size tags as can be seen in Figures 7, 8, 9, 10 curves for smaller tag sizes. As the analyzed frequency range is fixed for all tag sizes *i.e.* from 1-12 GHz, the reduction of size of the tag shifts its resonance spectrum to a higher frequency range outside of the analyzed frequency band. This causes lower detection accuracy for such cases. Therefore, we decided to remove these smaller fonts and rerun the test. Table 6 summarizes the detection accuracy results for these conducted experiments where these smaller sizes tags are removed in a subsequent fashion. The precision was increased to 92% by removing font sizes 16, 17, 18, and 19 from the data set. The analysis concludes that the overall test accuracy of all analyzed tags of different font sizes and font types can be enhanced by increasing the frequency range of analyzed spectrum.

In addition, the performance of the proposed DL model is characterized in terms of performance metrics such as sensitivity, specificity, F1 score, accuracy and false acceptance rate (positive) (FAR). These metrics are computed

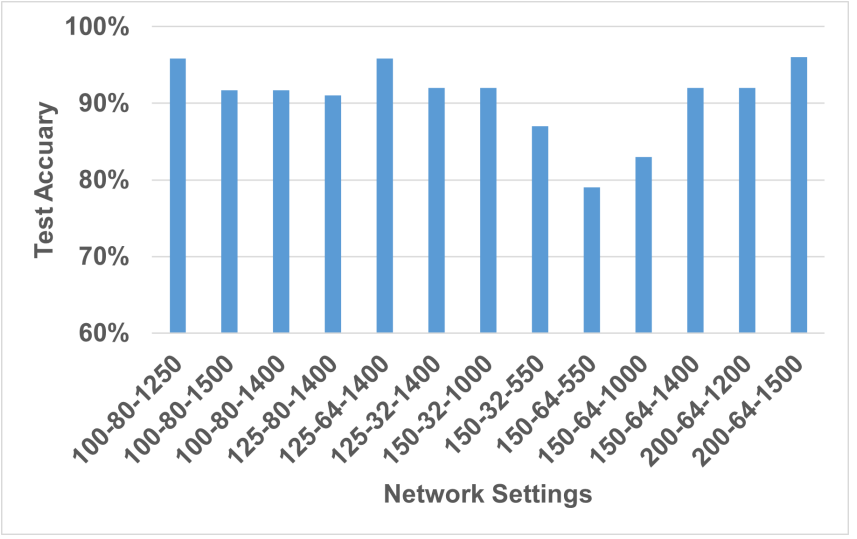

Figure 25: Test accuracy results of tag detection after removing four tags (ب, ج, ظ , و) from the data set in different hyper-parameters setting

Table 6
Summary of the effect of removing smaller font sizes on detection accuracy with a change in network settings (learning rate: 0.001)

Data Set	Fold	Test Accuracy
Remove Size 16,17,18,19	11	92 % ±5.7
Remove Size 16,17,18	35	85 %±2.4
Remove Size 19,20	35	85 % ±1.3

Table 7
Comparison of performance measure of different experiments

Dataset	Fold	Sensitivity	Specificity	F1-Score	Accuracy	FAR
All data Combined (Exp. 8)	10-Fold CV	79.7 % ±2.5 %	92 % ±1.9 %	79.5 % ±2.3 %	81.5 % ±1.2 %	8 % ±1.9 %
All data Combined (Exp. 9)	LOOCV	83.9 % ±3.1 %	82.6 % ±2.9 %	85.7 % ±2.9 %	88.8 % ±1.1 %	16.1 % ±3.1 %
All data without 4 unknown tags و , ظ, ج, ب	LOOCV	94.06 % ±7.5 %	92.05 % ±6.3 %	95.53% ±4.2 %	96 % ±5.1 % %	7.95 % ±6.3 %
All data without smaller font sizes (16, 17, 18)	LOOCV	91.07 % ±4.3 %	90.82 % ±2.1 %	79.88 % ±3.7 %	92 % ±5.7 %	9.18 % ±2.1 %
All data without smaller font sizes (19,20)	LOOCV	83 % ±1.9 %	82.96 % ±1.4 %	81.05 % ±2.9 %	85% ±1.3 %	17.04 % ±1.4 %

using the obtained true positive (TP), true negative (TN), false positive (FP), and false negative (FN) results. True positive (TP) is defined when the prediction is positive for the specific font type and size tag that must be identified. The negative predication for the non-presence of the specific font type and size tag is referred to as true negative (TN). False positive (FP) is referred to the case where the prediction of specific font type and size tag is positive while that tag is not present at the input and vice versa for the case of False negative (FN). These results are taken from the confusion matrix for each case. Table 7 presents the performance comparison of the all major conducted experiments.

It has been confirmed through the comprehensive analysis presented in Tables 5, 6, and 7 that the role of the appropriate choice of the classification model and the range of the RCS spectrum is vital to the increased precision of all tags. The number of resonance features is lower for the electrically smaller font size tags as compared to the larger size tags because of the analyzed frequency range of 1 to 12 GHz. This becomes the reason for the reduction in overall detection accuracy due to these tags, as summarized in Table 6. This limitation could be addressed by generating the new RCS characteristics of all tags for the wider frequency band.

The undertaken classification problem of Arabic RFID tags of various fonts and sizes is a multi-class classification problem that requires a classification technique that can learn long term dependencies. The proposed Bi-LSTM,

compared to other methods such as SVM, KNN, and decision trees, classified the data with much higher accuracy for such multiclass data. With optimized hyperparameters and removal of lower font size tags, a classification accuracy of 96% was achieved. However, LSTM takes longer to train and requires more memory. We were able to overcome this problem by running the model on a GPU. Also, LSTM models are sensitive to different random weight initializations and are easy to overfit. Additionally, the model may struggle to capture long-term dependencies in the data and may not work well with rare or out-of-vocabulary words, as we have noticed for the smaller font-size tags in our study. The model also may have difficulty dealing with imbalanced data, and may require a large amount of data to train effectively. These limitations could be addressed through the combinations of various solutions such as attention mechanism, pre-training, combining multiple Bi-LSTM models through ensembling with reduction of overfitting, tuning of model parameters using the global optimization technique, regularization, model interpretability, data augmentation, and other architectures as future work.

6. Conclusion

This work has proposed a robust reader (tag detection and classification) system for chipless Arabic RFID letter tags. The developed systems based on Bi-LSTM network can classify all 28 Arabic alphabet tags with three different font types (Arial, Calibri, and Times New Roman) and 13 different font sizes (16 mm - 28 mm with a step size of 1 mm). The study explained how the font size (or font type) of the tag could affect its signature resonance characteristics and makes the use of conventional phase/frequency modulation techniques cumbersome for all such letter tags. The proposed BiLSTM-based reader system analyzed the monostatic co- and cross-polar RCS characteristics of all tags for the accurate identification of each tag irrespective of its font type or size. As some Arabic letters differ by only point (s), testing of proposed network with combined data set of all fonts and sizes reported an accuracy of 89% that can be further enhanced to 96% with the abaltion of lower sizes tags. The compared conventional machine learning methods (SVM, Tree, KNN) produces very low accuracy (max. 27.4% with KNN) because of features mapping (resonances) of the tags with different shapes and sizes in the underline multidimensional classification problem. In addition to letter tags detection, the proposed approach has the potential for application in other areas, such as converting document images into digital documents, text detection in images, document / cheque security, product advertisements, and also for use in autonomous vehicles to read license plates.

References

[1] X. Fan, F. Wang, F. Wang, W. Gong, J. Liu, When rfid meets deep learning: Exploring cognitive intelligence for activity identification, IEEE Wireless Communications 26 (2019) 19–25.

[2] B. P. E. Alvarado Vásquez, F. Matía, A tour-guide robot: Moving towards interaction with humans, Engineering Applications of Artificial Intelligence 88 (2020) 103356.

[3] G. Kapoor, S. Piramuthu, Vulnerabilities in chen and deng's rfid mutual authentication and privacy protection protocol, Engineering Applications of Artificial Intelligence 24 (2011) 1300–1302. Infrastructures and Tools for Multiagent Systems.

[4] M. A. Islam, N. C. Karmakar, A novel compact printable dual-polarized chipless rfid system, IEEE Transactions on Microwave Theory and Techniques 60 (2012) 2142–2151.

[5] K. Choy, K. H. Chow, K. L. Moon, X. Zeng, H. C. Lau, F. T. Chan, G. Ho, A rfid-case-based sample management system for fashion product development, Engineering Applications of Artificial Intelligence 22 (2009) 882–896. Artificial Intelligence Techniques for Supply Chain Management.

[6] H. Rmili, B. Oussama, J. Yousaf, B. Hakim, R. Mittra, T. Aguili, S. Tedjini, Robust detection for chipless rfid tags based on compact printable alphabets, Sensors 19 (2019) 4785.

[7] L. M. Arjomandi, G. Khadka, Z. Xiong, N. C. Karmakar, Document verification: A cloud-based computing pattern recognition approach to chipless rfid, IEEE Access 6 (2018) 78007–78015.

[8] A. Attaran, R. Rashidzadeh, Chipless radio frequency identification tag for iot applications, IEEE Internet of Things Journal 3 (2016) 1310–1318.

[9] F. Paredes, C. Herrojo, F. Martín, 3d-printed quasi-absolute electromagnetic encoders for chipless-rfid and motion control applications, Electronics 10 (2021).

[10] C. Herrojo, F. Paredes, J. Mata-Contreras, S. Zuffanelli, F. Martín, Multistate multiresonator spectral signature barcodes implemented by means of s-shaped split ring resonators (s-srrs), IEEE Transactions on Microwave Theory and Techniques 65 (2017) 2341–2352.

[11] S. Jeong, J. G. Hester, W. Su, M. M. Tentzeris, Read/interrogation enhancement of chipless rfids using machine learning techniques, IEEE Antennas and Wireless Propagation Letters 18 (2019) 2272–2276.

[12] D. Nastasiu, R. Scripcaru, A. Digulescu, C. Ioana, R. De Amorim, N. Barbot, R. Siragusa, E. Perret, F. Popescu, A new method of secure authentication based on electromagnetic signatures of chipless rfid tags and machine learning approaches, Sensors 20 (2020) 6385.

[13] B. Aslam, U. H. Khan, M. A. Azam, Y. Amin, J. Loo, H. Tenhunen, Miniaturized decoupled slotted patch rfid tag antennas for wearable health care, International Journal of RF and Microwave Computer-Aided Engineering 27 (2017) e21048.

[14] H. Huang, L. Su, A compact dual-polarized chipless rfid tag by using nested concentric square loops, IEEE Antennas and Wireless Propagation Letters 16 (2017) 1036–1039.
[15] J. McVay, A. Hoorfar, N. Engheta, Space-filling curve rfid tags, in: 2006 IEEE Radio and Wireless Symposium, 2006, pp. 199–202. doi:10.1109/RWS.2006.1615129.
[16] R. Anee, N. C. Karmakar, Chipless rfid tag localization, IEEE Transactions on Microwave Theory and Techniques 61 (2013) 4008–4017.
[17] A. Vena, E. Perret, S. Tedjini, A fully printable chipless rfid tag with detuning correction technique, IEEE Microwave and Wireless Components Letters 22 (2012) 209–211.
[18] J. Yousaf, E. Almajali, M. E. Najjar, A. Amir, A. Altaf, M. Elahi, S. S. Alja'afreh, H. Rmili, Flexible, fully printable, and inexpensive paper-based chipless arabic alphabet-based rfid tags, Sensors 22 (2022).
[19] T. Singh, S. Tedjini, E. Perret, A. Vena, A frequency signature based method for the rf identification of letters, in: 2011 IEEE International Conference on RFID, 2011, pp. 1–5. doi:10.1109/RFID.2011.5764628.
[20] O. Boularess, L. Ladhar, A. Affandi, S. Tedjini, Analysis of rcs signatures of chipless rfid tags based on arabic alphabet letters with punctuation., Applied Computational Electromagnetics Society Journal 34 (2019).
[21] O. Boularess, H. Rmili, T. Aguili, S. Tedjini, Analysis of electromagnetic signature of arabic alphabet as rf elementary coding particles, Wireless Power Transfer 2 (2015) 97–106.
[22] L. Arjomandi, G. Khadka, N. Karmakar, mm-wave letter-based chipless rfid tags on cheap plastic substrates, 2020, pp. 1–4. doi:10.1109/IMWS-AMP49156.2020.9199710.
[23] M. Svanda, M. Polivka, J. Havlicek, J. Machac, Chipless rfid tag with an improved magnitude and robustness of rcs response, Microwave and Optical Technology Letters 59 (2017) 488–492.
[24] M. N. Zaqumi, J. Yousaf, M. Zarouan, M. A. Hussaini, H. Rmili, Passive fractal chipless rfid tags based on cellular automata for security applications, The Applied Computational Electromagnetics Society Journal (ACES) 36 (2021) 559–567.
[25] A. Vena, T. Singh, S. Tedjini, E. Perret, Metallic letter identification based on radar approach, in: 2011 XXXth URSI General Assembly and Scientific Symposium, IEEE, 2011, pp. 1–4.
[26] K. Issa, Y. A. Alshoudokhi, M. A. Ashraf, M. R. AlShareef, H. M. Behairy, S. Alshebeili, H. Fathallah, A high-density l-shaped backscattering chipless tag for rfid bistatic systems, International Journal of Antennas and Propagation 2018 (2018).
[27] O. Boularess, T. Aguili, J. Yousaf, H. Rmili, B. Hakim, S. Tedjini, Design of robust detection system for printable chipless rfid tag alphabet letters, in: 2019 IEEE 19th Mediterranean Microwave Symposium (MMS), 2019, pp. 1–4. doi:10.1109/MMS48040.2019.9157284.
[28] O. Boularess, L. Ladhar, A. Affandi, S. Tedjini, Analysis of rcs signatures of chipless rfid tags based on arabic alphabet letters with punctuation., Applied Computational Electromagnetics Society Journal 34 (2019).
[29] W. M. Adbulkawi, A.-F. A. Sheta, Printable chipless rfid tags for iot applications, in: 2018 1st International Conference on Computer Applications & Information Security (ICCAIS), IEEE, 2018, pp. 1–4.
[30] A. Chandio, G. Gui, T. Kumar, I. Ullah, R. Ranjbarzadeh, A. M. Roy, A. Hussain, Y. Shen, Precise single-stage detector, arXiv preprint arXiv:2210.04252 (2022) 1–33.
[31] W. Khan, K. Raj, T. Kumar, A. M. Roy, B. Luo, Introducing urdu digits dataset with demonstration of an efficient and robust noisy decoder-based pseudo example generator, Symmetry 14 (2022).
[32] B. Jiang, S. Chen, B. Wang, B. Luo, Mglnn: Semi-supervised learning via multiple graph cooperative learning neural networks, Neural Networks 153 (2022) 204–214.
[33] S. K. Lakshminarayanan, J. P. McCrae, A comparative study of svm and lstm deep learning algorithms for stock market prediction., in: AICS, 2019, pp. 446–457.
[34] A. Graves, M. Liwicki, S. Fernández, R. Bertolami, H. Bunke, J. Schmidhuber, A novel connectionist system for unconstrained handwriting recognition, IEEE transactions on pattern analysis and machine intelligence 31 (2008) 855–868.
[35] H. Sak, A. Senior, F. Beaufays, Long short-term memory recurrent neural network architectures for large scale acoustic modeling, Proceedings of the Annual Conference of the International Speech Communication Association (2014) 338–342.